論文

단계적 다섬유 Fragmentation 시험법을 이용한 복합재료의 계면적 특성에 대한 새로운 평가방법

박종만* · 김진원* · Koichi Goda**

A New Evaluation Method for Interfacial Properties of Composites using the Gradual Multi-Fiber Fragmentation Test

Joung-Man Park*, Jin-Won Kim* and Koichi Goda**

초 록

Fragmentation 시험법에 의한 섬유상 복합재료의 계면적 특성에 대한 새로운 평가방법이, 순차적으로 섬유간의 간격이 변하게 된 단계적 다섬유 복합재료를 사용하여 제시되었다. 섬유간의 간격이 증가함에 따라, 부서진 섬유들의 형상비는 감소하였으며, 섬유와 기지간의 계면전단강도는 증가함을 보여주었다. 섬유간 거리의 역수를 취했을 때에, 형상비와 계면전단강도 모두가 포화되는 값을 보여주었다. 이것은 단계적 다섬유 복합재료가 형상비에서의 상한값을 나타내고, 계면전단강도에서 하한값을 보여 준다는 것을 의미한다. 이 fragmentation 시험법은 복합재료의 평가에 새로운 방법이 될 수 있다. 왜냐하면, 이 두 한계값의 차이를 줄이는 것이 복합재료의 강화에 효과적이기 때문이다. 또한, 섬유 파괴점 부근에서의 섬유응력 분포와 위의 결과를 관련시키기 위해 탄성-소성 유한요소 해석이 행해졌다. 단계적 다섬유 복합재료 시험에서 얻어진 한계값은 그룹형태의 다 섬유 파괴에 의해 야기된 응력집중과 밀접하게 관련되어 있다는 것이 입증되었다.

ABSTRACT

A new evaluation method for the interfacial properties of fibrous composites based on a fragmentation technique is proposed by using the gradual multi-fiber composite, in which the inter-fiber spacing is gradually changed. The results showed that as the inter-fiber distance increased, the aspect ratio of broken fibers decreased while the interfacial shear strength between the fiber and matrix increased. When the reciprocal of the inter-fiber distance was taken for the above relations, both the aspect ratio and interfacial shear strength showed a saturated value. This means that the gradual multi-fiber composite indicates an upper bound in aspect ratio and a lower bound in interfacial shear strength, while the single fiber composite shows a lower bound in aspect ratio and an upper bound in interfacial shear strength. It was concluded that this fragmentation test could be a new method for composite evaluation, since reducing a difference between these two bounds is effective for composite strengthening. In addition an elastoplastic finite element analysis was carried out to relate the above results with fiber stress a distribution around fiber breaks. It was proved that the bound obtained in the gradual multi-fiber composite test is closely related to stress concentrations caused by a group of multi-fiber breaks.

*경상대학교 고분자공학과, 항공기부품기술연구센타
*경상대학교 고분자공학과 대학원
**Dept. of Mechanical Engineering, Yamaguchi University, JAPAN

INTRODUCTION

Interfacial adhesion is one of the most important factors to determine properties of fibrous composite materials. To evaluate the interfacial adhesion of the composites, micro-specimens embedding one or more fibers have been used for micromechanical tests, which are to evaluate the interfacial properties, such as interfacial shear strength (IFSS) between the fiber and matrix and aspect ratio of broken fibers. Some conventional techniques for measuring the IFSS include the single fiber microdroplet test [1, 2], single fiber composite (SFC) test [3-5] and microindentation test [6].

The single fiber microdroplet test (which is also known as the single fiber pull-out test [1, 2, 7]) can measure the interfacial shear load by pulling out a fiber from a lump of the matrix. This test was shown to be the best method to measure the IFSS, because it can directly measure the interfacial shear load between the fiber and matrix independent of their properties. In the microindentation test, a rigid indenture is pushed down on a cross-sectional area of the fiber in a thin composite plate. The load is repeatedly measured until debonding. These two tests are essentially identical in a point that the interfacial shear load can directly be detected.

The SFC test (also known as the fragmentation test), originally proposed by Kelly-Tyson [8] for metal matrix composites, can provide abundant statistical information from only several specimens as well as the interfacial failure modes and the IFSS. Based on an equilibrium condition in an axial fiber stress and matrix shear stress, Kelly and Tyson showed that the IFSS, τ is given by,

$$\tau = \frac{\sigma_f \cdot d}{2 \cdot \bar{l}_c} \tag{1}$$

where, d is the fiber diameter, σ_f is the fiber fracture strength, and $\bar{l}_c$ is the average critical fragment length. Since the actual fragment length and the fiber strength are not constant but are strongly dependent on the gauge length, eq. (1) can be modified as,

$$\tau = \frac{\sigma_f \cdot d}{2 \cdot \bar{l}_c} \cdot K \tag{2}$$

where, σ_f is the fiber tensile strength at a gauge length equal to the mean fragment length, and K is a coefficient, which depends on the variation of the fragment length [9]. If the fragment length varies between $l_c/2$ and l_c, K=0.75 can be taken as a mean value. Since the fragment length is distributed experimentally, Drzal et al. [10] proposed the following equation by taking the Weibull statistics into account,

$$\tau = \frac{\sigma_f}{2\alpha} \cdot K, \quad K = \Gamma\left[1 - \frac{1}{\beta}\right] \tag{3}$$

where β is the shape parameter, α is the scale parameter in the Weibull distribution and Γ is the Gamma function.

Since the SFC technique considers only an interface around a single fiber, it can not match well with the interfacial properties of real composites in which the fibers interact with each other. Therefore, a composite specimen with a small number of fibers was developed to model more practically the composites [11-14]. This composite is called the multi-fiber composite (MFC), which are generally prepared with equal inter-fiber separation (hereafter, this is referred to as 'the regular MFC'). Thus the regular MFC test has been used for evaluating the interfacial properties with the fiber to fiber interaction as a function of the inter-fiber distance.

The gradual MFC proposed here is characterized by gradually changing the inter-fiber spacing. In the regular MFC with small inter-fiber spacing, the fiber to fiber interaction must be strong. On the other hand, in the SFC there is no interaction

between fibers. It is expected that, therefore, in the gradual MFC test both fragmentation properties obtained in the SFC and the regular MFC tests may appear at the same time. In other words a change of the interaction would be found out in only a kind of specimen. The main objective of this study is to propose a new evaluation method, which takes the effect of interaction between fibers into the interfacial properties by using the gradual multi-fiber fragmentation technique.

EXPERIMENTAL

Materials

Fiber E-glass fiber with diameter of 30.3 ㎛ was used without sizing treatment, which was supplied from Dow Corning Co. The strength of the glass fiber was measured by the tensile test using single fiber specimens. The elastic moduli and the average density of the glass fiber were 58.6 GPa and 2.55 g/cm^3, respectively. The tensile properties of the glass fiber were measured before preparing the micro-composite specimens.

Polymer Matrix The MFCs were prepared with epoxy resin (YD-128), which was provided from Kukdo Chemical Co. Epoxy resin is based on diglycidylether of bisphenol-A (DEGBA). Jeffamine D400 and D2000 based on polyoxypropylenediamine were used as curing agents and purchased from Huntsman Petrochemical Co. Flexibility of the specimens was controlled by adjusting the relative proportions of D400 *versus* D2000 in the curing mixture for the ductile epoxy matrix. The chemical structure of curing agents is as follows:

$$H_2N-CH_2-\underset{\displaystyle CH_3}{\underset{|}{CH}}-(OCH_2-\underset{\displaystyle CH_3}{\underset{|}{CH}})_x-NH_2$$

where, x is average 5.6 for D400 and 33.1 for D2000, respectively. It was precured for 2 hours at 80 ℃ and then postcured for 1 hour at 120 ℃. The *m*-phenlenediamine (*m*PDA) curing agent was also used for the comparison.

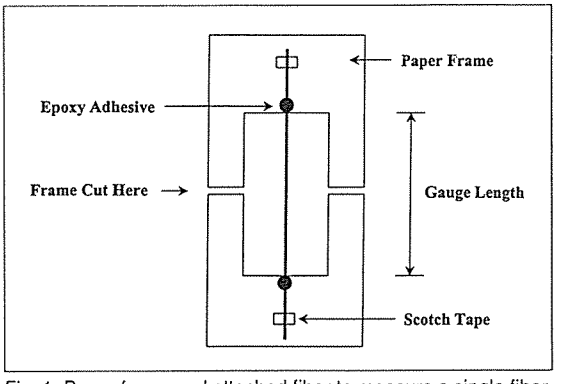

Fig. 1. Paper frame and attached fiber to measure a single fiber tensile test.

Methods

Measurement of Single Fiber Tensile Properties Tensile strength of most ceramic fibers such as glass fibers is known to be significantly dependent on the gauge length, due to the random distribution and variant sizes of flaws along the fiber surface. About fifty specimens in each gauge length were tested. The gauge lengths of testing specimen were 2, 5, 10, 20, and 100 mm, respectively. An average diameter of fifty glass fibers was measured by an optical microscope (Nikon model: HEX-DX) attached a calibrated eye's piece. The diameter of a fiber was measured at three different points, and the minimum value of the measured diameter was chosen.

A single fiber was placed on a paper frame and then was fixed by Scotch tape in the center line on both ends. The epoxy adhesive was used to fix the fiber in place (Figure 1). Tensile strength was measured using the universal testing machine (Lloyd instruments Ltd Co., LR-10K) attached with 100 N load cell. The cross-head speed was 0.5 mm/min.

Preparation of the Regular and the Gradual MFCs The regular- and gradual MFC spec-

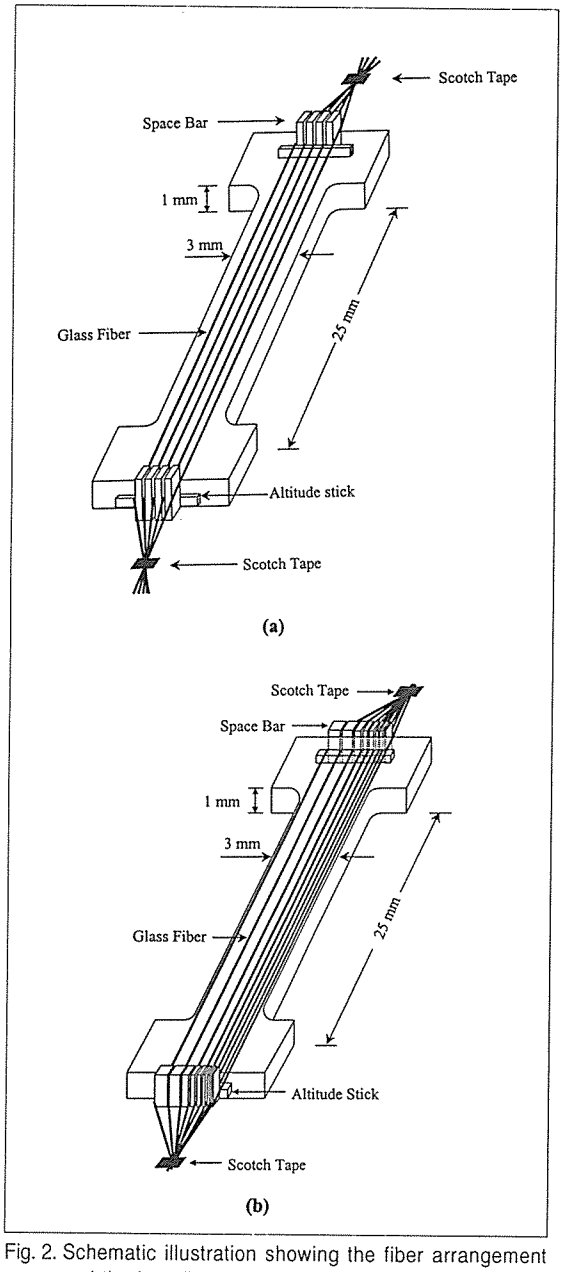

Fig. 2. Schematic illustration showing the fiber arrangement and the inter-fiber separation in two-typed composites: (a) the regular multi-fiber composite; and (b) the gradual multi-fiber composite.

imens were prepared as shown in Figure 2 (a) and (b), respectively. Space bars serving as an inter-

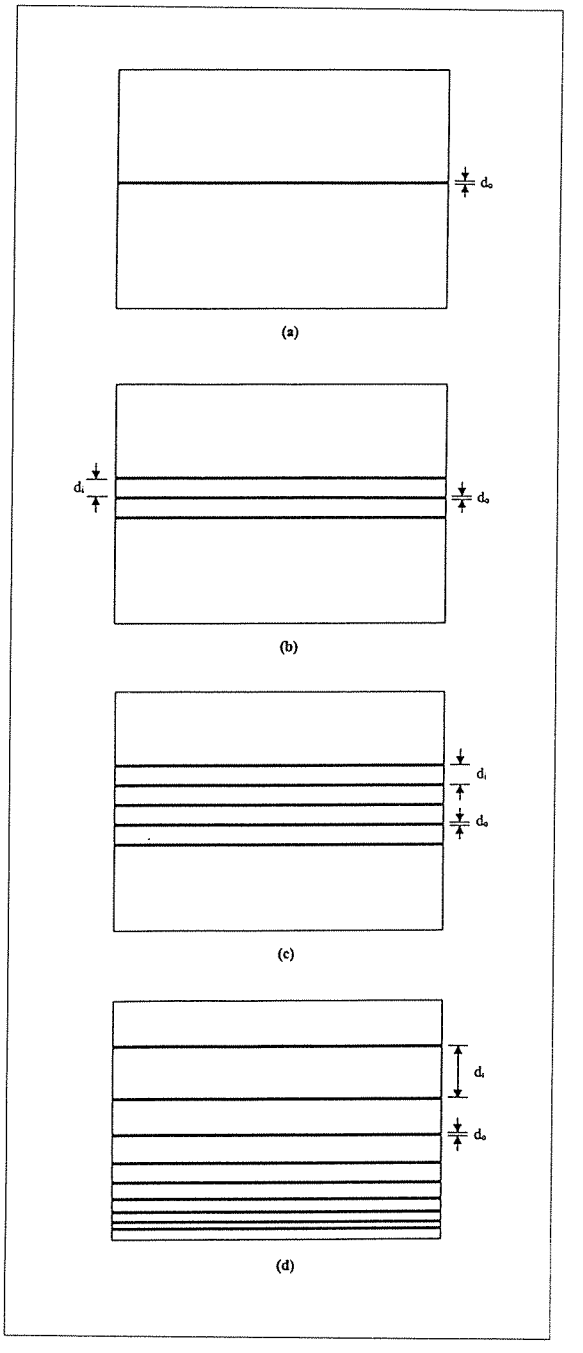

Fig. 3. Configuration of specimens for the single-fiber or the multi-fiber fragmentation test:
(a) single-fiber; (b) regular three-fibers; (c) regular five-fibers; (d) gradual multi-fiber reinforced composites.

fiber separation were equipped. After multi-fiber was laid down between space bars, the end of a fiber was fixed by Scotch tape. The dimension of two-typed multi-fiber specimens was 3 mm wide, 25 mm gauge length, and 1 mm thickness. Figures 3 (a) to (c) represent the configurations of the single- and the regular MFCs with three and five fibers, where all inter-fiber spacing was the same magnitude. Figure (d) shows the configuration of the gradual MFC specimen, in which the inter-fiber spacing, d_i was increased gradually with suitably-multiple distance of fiber diameter as follows: 1 time: 30 μm; 2 times: 60 μm; 3 times: 90 μm; 4 times: 120 μm; 5 times: 130 μm; 7 times: 210 μm; 10 times: 300 μm; and 15 times: 500 μm, respectively.

Multi-fiber was embedded in the flexibilized epoxy using Jeffamine curing agents on a silicon mold. After these specimens were left at room temperature for 24 hours, they were precured at 80 ℃ for 2 hours and postcured at 120 ℃ for 1 hour.

After the fiber position and the straightness were checked carefully with an optical microscope, the unsuitable specimens were discarded. After the specimen was taken out from the mold, the specimen was polished by the standard metallographic technique to obtain the smooth surface and same thickness. Bulk epoxy specimens were tensile-tested by universal testing machine (10 KN load cell, 1 mm/min. cross-head speed rate). A set consisting of three specimens was tested and the stress *versus* the strain curve was drawn.

For preparing the MFCs, the degassed resin mixture was cast into a silicon mold. Each fiber was positioned at a half depth of the specimen thickness. After curing, the specimens were transparent enough to observe the microfailure modes. The specimens were tested after aging for 3 days at room temperature and humidity to equilibrate.

IFSS Measurement IFSS of the MFCs was investigated by the multi-fiber fragmentation test. The interfacial failure occurring on the individual fiber was observed *via* an optical microscope with a specially-designed tensile machine. During testing, the specimen was stressed incrementally and the fibers were fractured into small segments within matrix. As the tensile stress was applied further, the fracture process continued until no longer fracture occurred in the fiber. At this strain a fragment length is called as a critical fragment length, *lc*. The critical fragment length of the individual fiber was measured and their microfailure modes were observed *via* a polarized-light microscope.

The classical relationship among the fiber tensile strength, the critical fragment length to diameter ratio (i.e., aspect ratio, *lc* /d) and IFSS, τ was given by Kelly-Tyson as in the eq. (1). Widely-distributed τ values are obtained as a result of the random distribution and the heterogeneity of the flaws in fibers. The data for the both fragment length and the fiber strength may be approximated by Weibull distribution [15] and these distributions can be combined to calculate IFSS. The cumulative probability of failure of a fiber length l loaded to stress level σ is given by [16, 17],

$$F = 1 - \exp\left\{-l\left(\frac{\sigma}{\sigma_0}\right)^m\right\} \tag{5}$$

where σ_0 is the scale parameter, m is the shape parameter (so-called the Weibull modulus), the slope of a cumulative distribution, and F is assigned as,

$$F = \frac{i}{N+1} \tag{6}$$

where N is the total number of the fiber fragments, and i is the rank number. To evaluate the parameters, m and σ_0, eq. (6) can be rearranged into a linearized form as,

$$\ln[-\ln(1-F)] = m\ln t - m\ln\sigma_0 \quad (7)$$

Thus, the plot of ln [-ln (1-*F*)] *versus* ln (aspect ratio) yields a straight line which slope and the intercept yields m and σ_0, respectively. IFSS can be calculated by eq. (3).

To know the tensile strength at the critical length, a direct tensile test at such a short length can result in experimental difficulties [18]. Fiber strengths are usually determined by the macroscopic gauge lengths, and then with subsequent extrapolation to smaller gauge length using Weibull weakest link rule. It was calculated from the extrapolation of the fiber strength measured at an individual gauge length. The fiber strength σ_f at the critical fragment length is

$$\sigma_f = \sigma_{f_0} \cdot \left(\frac{\overline{l_c}}{l_o}\right)^{-\frac{1}{m}} \quad (8)$$

where, σ_{f_0} is fiber strength at gauge length, l_0.

RESULTS

Statistical and Mechanical Properties of Fiber and Matrix Table 1 shows the average tensile strengths and elongation of a single glass fiber for the various gauge lengths. As the gauge length increased, both the average tensile strength and the elongation decreased. This is because a severer flaw on the fiber surface or a larger internal defect exists stochastically in the longer gauge length. Figure 4 shows the Weibull parameters for the tensile strength of the fiber obtained from the Weibull statistical analysis. The result shows that the scale parameter increased as the gauge length decreased. This is also due to the same reason as the changes of the average tensile strength and elongation. On the other hand, the shape parameter slightly increased with a decrease in gauge

Table 1. Tensile properties and their Weibull parameters of single glass fiber (diameter: 30.3 μm) with various gauge lengths.

Gauge Length (mm)	No. of Specimen (EA)	Diameter (μm)	Elongation (%)	Tensile Strength (MPa)	Scale Parameter (α)	Shape Parameter (β)
2	40	30.3 (1.7)[a]	11.4 (2.5)	2487	2619	5.1
5	44	30.1 (1.1)	5.7 (1.2)	2206	2483	4.1
10	45	30.3 (1.3)	4.9 (1.4)	1956	2031	4.3
20	37	30.1 (1.0)	2.8 (0.9)	1483	1803	3.7
100	42	30.6 (2.0)	1.4 (0.4)	1029	1215	3.8

a Standard deviation
* Used estimator is $F(X_i)=i/(N+1)$

Table 2. Mechanical properties of the epoxy specimens with various curing agents.

Curing agent	Tensile Strength (MPa)	Modulus (GPa)	Strain of Breakage (%)
mPDA	84.2 (7.0)[a]	2.52 (0.4)	5.5 (0.8)
D400	41.1 (3.8)	2.00 (0.2)	8.8 (2.6)
D400 + D2000[b]	35.8 (6.6)	1.76 (0.2)	40.5 (1.9)
D400 + D2000[b]	24.6 (1.9)	1.56 (0.2)	66.6 (5.2)

a Standard deviation
b Different mixing ratio
- Each four specimens were used.

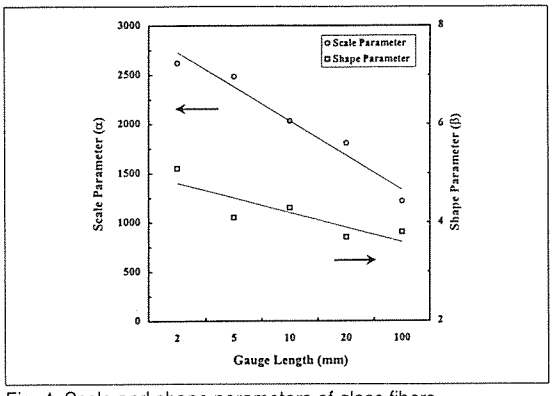

Fig. 4. Scale and shape parameters of glass fibers (diameter: 30.3 μm) with various gauge lengths.

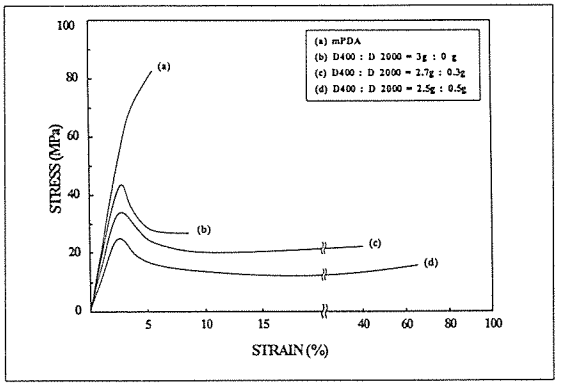

Fig. 5. Plot of stress-strain curve for the dogbone-shaped epoxy specimens using four different curing agents: (a) *m*PDA; (b) D2000: 0 g; (c) D2000: 0.3 g; (d) D2000: 0.5 g.

length, despite that this parameter is often recognized to be a material constant. Such a change of the shape parameter is often caused by the bimodality of the strength distributions of a surface flaw and an internal defect [19]. In this point the estimates of shape parameter obtained here are consistent. Also the change may be interpreted by the clamp effect which appears especially in short gauge length [20].

Table 2 shows the tensile properties of epoxy specimen with various curing agents, and their stress-strain curves are shown in Figure 5. Epoxy (a) using *m*PDA hardener was the most rigid and brittle and showed the highest tensile strength, modulus and the smallest elongation. As the amount of the flexible curing agent increased, the tensile modulus decreased whereas the elongation increased. Epoxy (c) and (d) showed to be more ductile than others, with higher elongation and uniform deformation behavior without necking. In the epoxies (c) and (d), the former indicated higher tensile modulus than the latter. At highly-elongated range epoxy (d) showed a slightly increasing trend because of the strain hardening. For the matrix used here it is necessary to posses a sufficient ductility which can yield a saturated multiple fiber-break state along the fiber axis while straining. Thus, epoxy (c) was chosen as the matrix for preparing the MFC specimens.

Microfailure Modes in the Regular and the Gradual MFCs Figure 6 shows the shear stress birefringence in the matrix around the break points in (a) the regular and (b) the gradual MFCs with polarized-light. In Figure 6(a), distinct fiber fracture modes were exhibited and all fibers were broken successively in a series around neighboring fibers. It is considered because the fracture energy caused by a fiber break affected intensively adjacent fibers. Such a breaking process was observed throughout the testing specimen. In Figure 6(b), on the other hand, breaking positions of the individual fiber were rather random or irregular.

Figure 7 shows a series of the birefringence pattern of fiber fracture modes in the gradual MFC. When the tensile stress was applied, a fiber break occurred at the position of a narrow inter-fiber spacing in the initial stage of the figure (a). It may be because the effect of shrinkage acts in the matrix among the multi-fibers particularly with narrow spacing, which is often caused by the difference between Poisson's ratios of the fiber and matrix. At a breaking position, stress whitening was observed with high angle. This angle became lower while the tensile load is further increased, as shown in the figure (b). Two matrix cracks at closely placed two fibers were overlapped and the

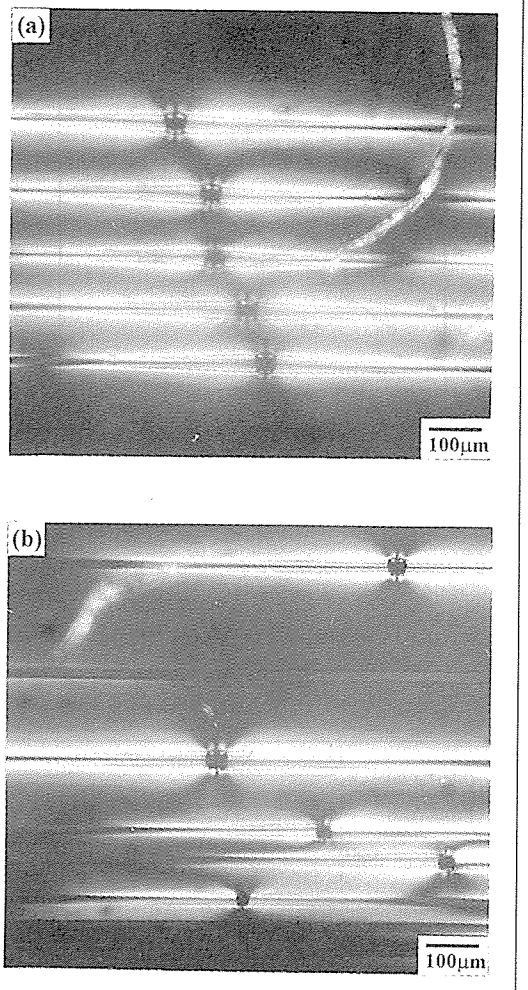

Fig. 6. Optical photographs of the fiber fractures in multi-fiber composites with a polarized-light: (a) the regular-; (b) the gradual-.

cone-shaped crack was propagated to perpendicular direction of the fiber axis. Crack gap increased further with an increase in elongation. One of the significantly-large crack cones may result in a catastrophic failure of the specimen at higher strain state. In any case, after a fiber was broken, fiber breakage did not occur along the same fiber axis, but occurred at the weak section of adjacent

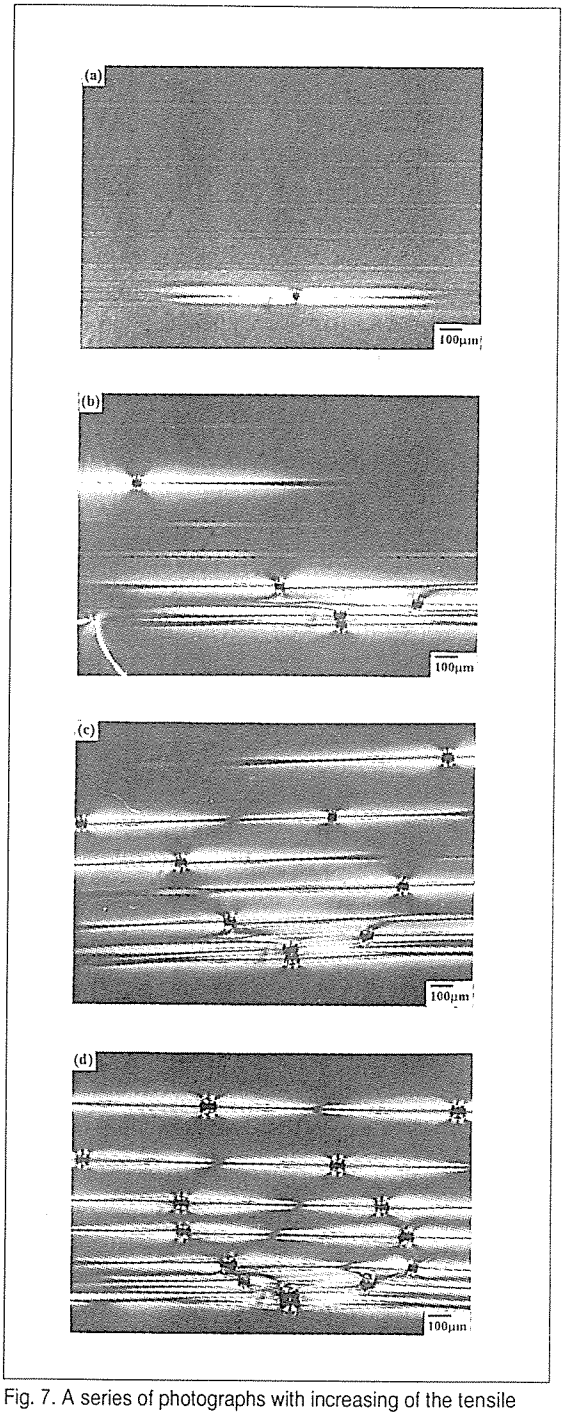

Fig. 7. A series of photographs with increasing of the tensile strain: (a) 1 % strain; (b) 4 % strain; (c) 6 % strain; (d) 10 % strain.

fibers.

As the strain is further increased, more fiber breakage at the wide spacing occurred as shown in the figures (c) and (d). The final number of fiber breakage at wide inter-fiber spacing was more than that at narrows inter-fiber ones. In the narrow spacing, many failures exhibited a continuous steps-like shape with increasing the strain. In the narrow inter-fiber spacing a fiber breakage is considered to cause not only subsequent matrix cracking but neighboring fiber breaks, because a stress concentration occurs around its breakage point. Thus, in the narrow separation any breakage does not accompanied along the same fiber axis. On the other hand, in the wide inter-fiber spacing fiber breakage points are irregular because the effect of the stress concentration is considered to be less effective. It is concluded from the above that fiber fracture process is significantly dependent on the degree of inter-fiber spacing.

Aspect Ratio and IFSS of SFC and Regular MFC The interfacial properties of the SFC and regular MFC using the fragmentation technique are given in Table 3. Figure 8 shows the average aspect ratio and their IFSS in the regular MFCs consisting of three and five fibers with a change in inter-fiber separation. As the inter-fiber separation increased, the mean fragment length and aspect ratio decreased whereas the IFSS increased. Since in the narrower separation the stress concentration due to a fiber break can more intensively affect the adjacent fibers, the specimen can include easily crack propagation. That is to say, the fragment length in the narrower separation is further increased. Again we realize here that inter-fiber spacing plays an important role in determining the interfacial properties in fibrous composites.

Figure 9 shows the effect of the number of embedded fiber in the SFC and the regular MFC on the IFSS. The more number of embedded

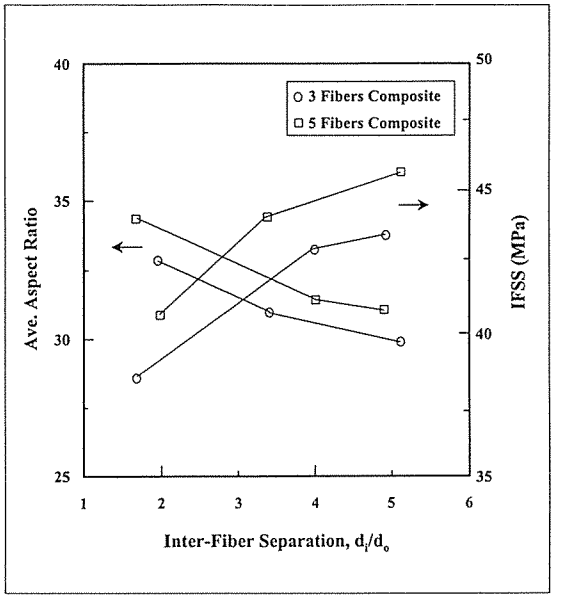

Fig. 8. Effect of the inter-fiber separation on the average aspect ratio and IFSS in the regular three- and five-fiber composites.

Table 3. Value of the interfacial properties resulted from the single fiber and regular multi-fiber fragmentation test.

Interfacial Properties	No. of Embedded Fibers						
	1(EA)	3 (EA)			5 (EA)		
Fiber Separation, d_i/d_o[a]	-	2.0	3.4	5.1	1.7	4.0	4.9
Ave. Fragment Length(mm)	0.85	1.0	0.9	0.9	1.0	1.0	0.9
Ave. Aspect Ratio	27.9	32.8	31.0	29.9	34.4	31.4	31.3
IFSS (MPa)	49.5	40.8	44.2	45.8	38.6	43.1	43.6

a d_i and d_o are inter-fiber spacing and fiber diameter, respectively.

fibers, the lower the IFSS. Because the MFC can contain multiple fiber-break causing crack propagation and results in a catastrophic failure of the specimen. On the other hand, the SFC showed considerably-high IFSS, as compared to that of the regular MFC. It may be because the SFC can extend higher elongation until fracture due to the absence of multiple fiber-breaks. In addition, there is no stress dissipation toward adjacent fibers.

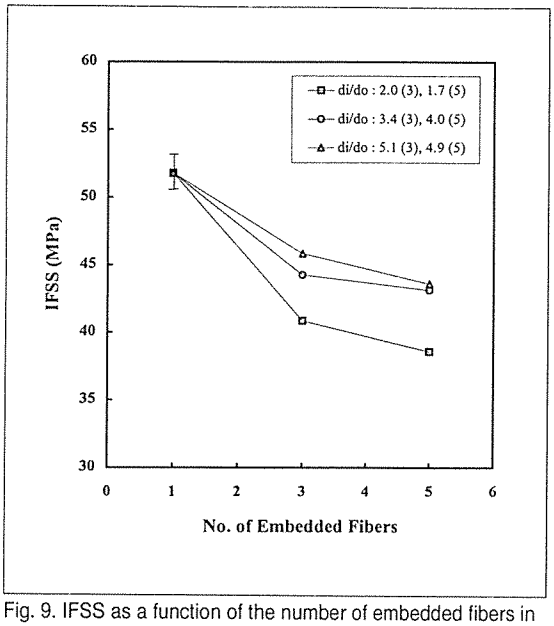

Fig. 9. IFSS as a function of the number of embedded fibers in the single-fiber and the regular multi-fiber composites.

It may be concluded from the above that the SFC specimen can exhibit the highest value in IFSS and the lowest one in aspect ratio of all fragmentation composite specimens. Such an interpretation is also implied by Z. F. Li et al. [11].

Aspect Ratio and IFSS of Gradual MFC

The interfacial properties of the gradual MFCs using the fragmentation technique are given in Table 4. Figure 10 shows (a) the average aspect ratio and (b) IFSS with an increase in the inter-fiber separation. As the inter-fiber separation increases, the average fragment length and aspect ratio decreased whereas the IFSS increased. These have the same tendency as the results obtained in the regular MFC test. Although these changes are apparently almost linear for both 6 and 12 % elongation, an unconventional aspect was found out by taking the reciprocal of d_i/d_o. Figure 11 shows the relations of the aspect ratio and IFSS to d_i/d_o. As the d_i/d_o increased, that is, as the inter-fiber spacing decreased, the aspect ratios for 6% and 12% elongation first increased and then saturated around 40 and 45, respectively. These saturated values were approximately similar with the values of the y-intercept in the Figure 10(a). The IFSS for 6% and 12% elongation first decreased and then saturated similarly around 27.5 MPa and 32.5

Table 4. Values of the interfacial properties resulted from the gradual multi-fiber fragmentation test.

	Order of fibers	1	2	3	4	5	6	7	8	9
Elongation	Fiber Separation (d_i/d_o)[a]	0.9	0.8	1.9	4.0	4.3	7.1	8.9	15.7	-
6 %	Fragment Length (mm)	1.4	1.5	1.4	1.4	1.3	1.3	1.2	1.2	1.1
		(0.3)[b]	(0.4)	(0.2)	(0.2)	(0.3)	(0.2)	(0.1)	(0.2)	(0.1)
	Aspect Ratio	42.1	49.4	46.4	44.5	42.8	45.9	39.7	36.9	37.5
		(9.3)	(12.9)	(7.2)	(5.2)	(8.6)	(5.4)	(3.2)	(6.3)	(4.4)
	IFSS (MPa)	28.8	26.7	27.6	28.6	30.6	29.4	32.6	36.2	35.2
		(6.8)	(9.2)	(5.7)	(4.0)	(7.0)	(4.7)	(3.3)	(6.7)	(5.3)
12 %	Fragment Length (mm)	1.2	1.3	1.4	1.3	1.3	1.2	1.1	1.0	1.0
		(0.1)	(0.2)	(0.1)	(0.1)	(0.2)	(0.2)	(0.1)	(0.2)	(0.1)
	Aspect Ratio	39.4	40.2	42.5	41.4	41.1	38.1	36.3	33.5	33.2
		(1.8)	(6.5)	(4.0)	(3.1)	(6.2)	(7.5)	(3.3)	(6.0)	(2.8)
	IFSS (MPa)	32.7	32.6	31.1	31.4	31.6	35.3	36.4	40.8	40.4
		(1.8)	(5.7)	(3.5)	(2.0)	(5.6)	(8.2)	(3.9)	(8.5)	(3.9)

a d_i and d_o are inter-fiber spacing and fiber diameter, respectively.
b Standard deviation (SD)
* Glass fiber diameter : 30.0 μm

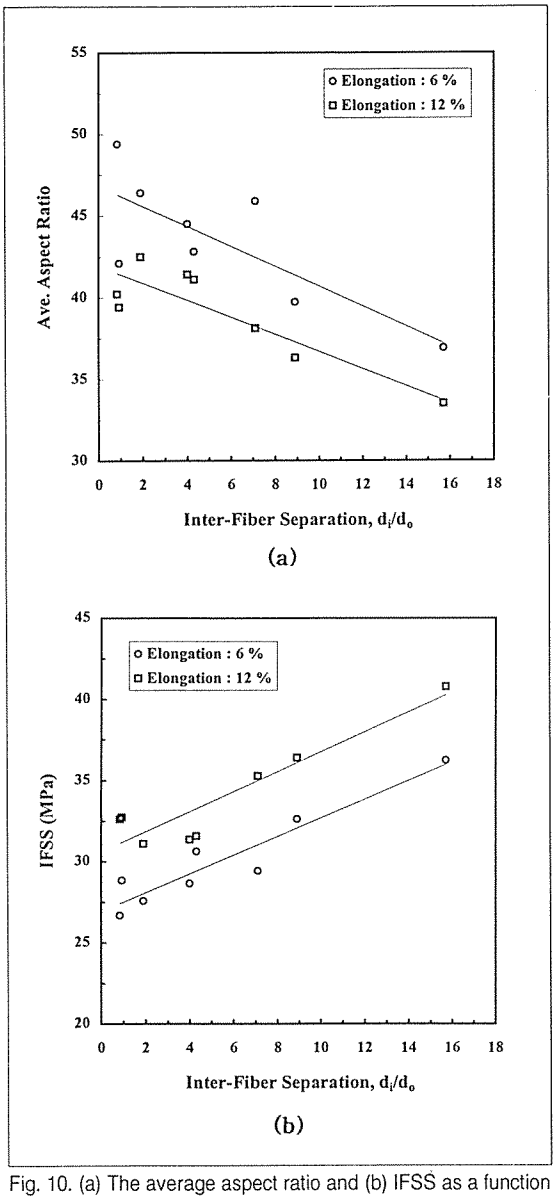

Fig. 10. (a) The average aspect ratio and (b) IFSS as a function of the inter-fiber separation at 6 % and 12 % elongation.

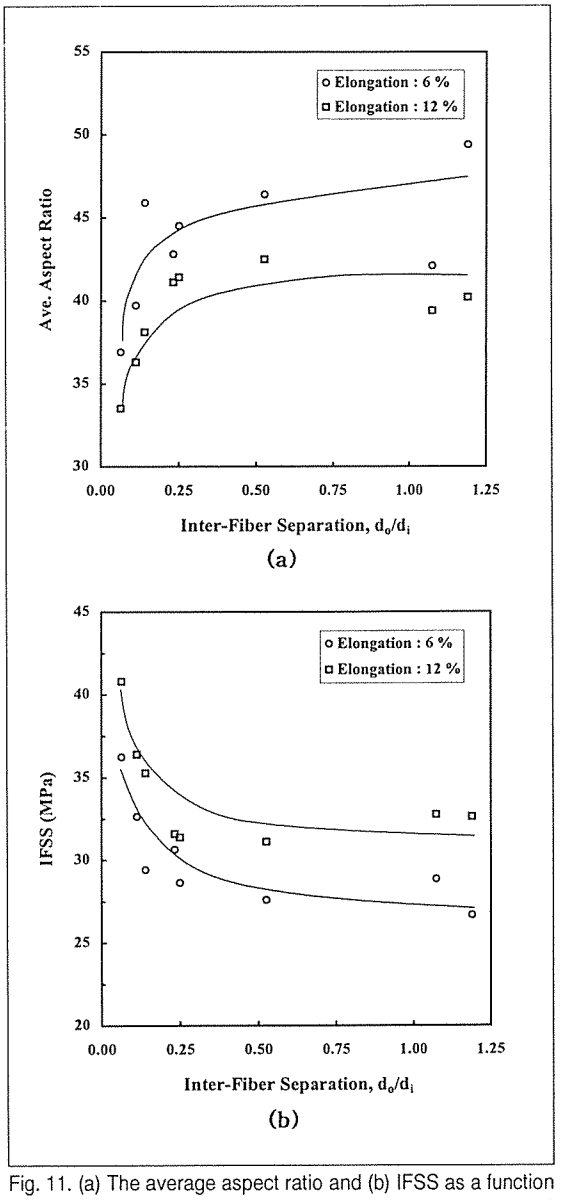

Fig. 11. (a) The average aspect ratio and (b) IFSS as a function of the reciprocal of the inter- fiber separation at 6 % and 12 % elongation.

MPa, respectively. These results mean that, while the SFC test can estimate an lower bound in aspect ratio and an upper bound in IFSS, the gradual MFC test can conversely estimate an upper bound in aspect ratio and an lower one in IFSS. Needless to say, the existence of such another bound is easily found out, because the gradual MFC can yield a change in fiber stress distribution around the break point(s), which is caused by the gradually changed inter-fiber separation. In the regular MFC test, however, many and various specimens would be necessary to find the opposite

bound.

If the upper bound in aspect ratio or lower bound in IFSS approaches nearer to the opposite bound, the strengthening effect of this composite is considered to become higher. Because, the interfacial properties without interaction between fibers, as given in the SFC test, are the best. We should choose a combination of fiber and matrix giving a smaller difference between the two bounds at composite production. Advanced composite materials such as carbon-fiber-reinforced composites are generally imposed to have high fiber volume fraction of 50% to 60%. Since in such composites the effect of stress concentration is positively exhibited, an evaluation method including an interaction between fibers should be developed. In this point the gradual multi-fiber fragmentation test is concluded to be a new evaluation method for fibrous composites. To estimate accurately the proposed new bound, we will further investigate the more suitable configuration for the gradual MFC specimen, by changing variously the number of fibers, the degree of interfacial spacing and so on.

DISCUSSION

As mentioned earlier the multi-fiber with a narrow inter-fiber spacing are successively broken, because of stress concentration. On the other hand, the fibers with a wide spacing are irregularly broken, irrespective of positions of breakage points. And it was experimentally proved that the broken fibers with a narrow spacing are larger in aspect ratio than the broken ones with a wide spacing. What fiber stress distribution brought such a difference? In this section the fiber stress distribution around broken fiber(s) is discussed from a mechanical viewpoint using an elastoplastic finite element analysis.

Analytical method Figure 12 shows the finite element mesh of the gradual MFC specimen used in the present study. The FE mesh consists of a two-node line element and a four-node isoparametric element under plane stress condition. The line element and the isoparametric element express the fiber and the matrix, respectively. Hereafter we call them the fiber element and matrix element, respectively. The fiber element is characterized by being incorporated into two nodes along y-axis of the matrix element, as shown in the figure [21]. According to the micromechanical finite element analysis for a short fiber embedded in an elastoplastic material, the stress components except for the normal stress along the fiber direction can be almost neglected [22]. It is expected that, therefore, the number of nodes is economized. It is also noted that this model can estimate the normal stress component acting on the matrix, which has been neglected in the conventional shear-lag model [23]. It is then assumed that the fiber element behaves linear-

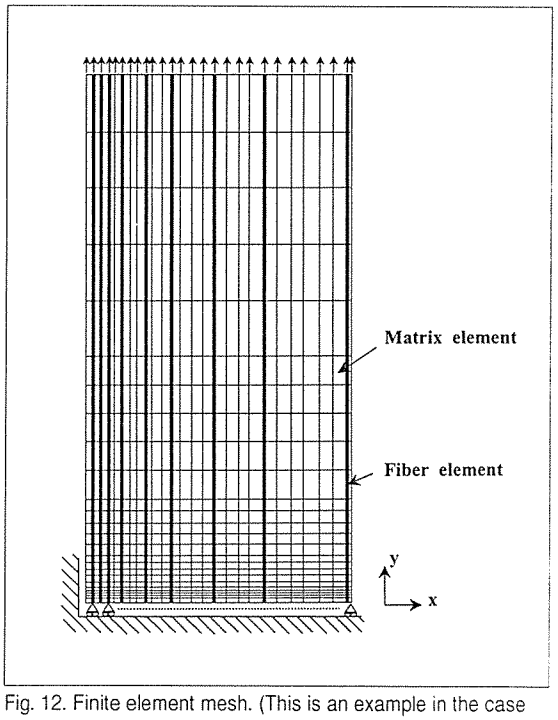

Fig. 12. Finite element mesh. (This is an example in the case that a support is removed at the second-arrayed fiber from the left.)

elastically up to its strength level and loses statically its deformation resistance immediately after achieving the level. The matrix element is assumed to be an elastoplastic body following the n-power hardening plasticity rule. For simplicity the matrix is assumed to be without fracture of itself. Due to this, stress concentration state around multiple fiber-break points may be underestimated to some degree in comparison with practical state. However, the objective of this chapter is to understand a relative stress distribution of the fiber under the gradually changed inter-fiber separation. The yield stress, n-power exponent and plastic coefficient of the matrix were approximated by the least square method from the stress-strain curve of Figure 5(c). The FE mesh includes nine fibers which is the same number as the gradual MFC specimen used here. The inter-fiber distances were also meshed following the experimental distances. The thickness of matrix element was set to 0.2 mm to limit the effect of fiber breakage to some extent. The present FE mesh is a half length of the composite specimen, and composed of 225 fiber elements, 650 matrix elements and 702 nodes. Material constants used in this study are shown in Table 5.

The present calculation method is as follows: First, displacement increments along y-axis direction at each end are repeatedly applied in tensile direction as boundary condition. If the fiber stress on the local coordinate achieves its strength, the fiber should be broken. In this study a support at the fixed end of the mesh were intentionally removed to simulate the breakage. This means that it occurs at the center of the fiber from symmetry in stress distribution. Then a support load was incrementally released in tensile direction from the end as boundary condition. The fiber strength level used here was set to 980.0 MPa, which was decided from the average in the minimum distribution of the Weibull function[*1].

Analytical results Figure 13 shows the results of stress analysis obtained in the present FEM. In the figures all the stresses are non-dimensionalized by dividing the analyzed stresses by the strength level of 980.0 MPa. The figure (a) shows that the axial stresses in the 1st and 2nd fibers are redistributed, after the 2nd fiber is broken. In the 2nd fiber the stress is recovered immediately apart from the broken point. A length over which the fiber stress is less than $\phi\delta_{app}$, may be considered ineffective for strengthening the composite [24]. (where δ_{app}, is the fiber stress acting at remote points, and ϕ is defined as 0.95 in this study). This length is called the ineffective length, and evaluated as a parameter for indicating strength efficiency for fibrous composites. Since the fragment length in the fragmentation technique is substantially related with the ineffective length, the aspect ratio is corresponding to this length. In Figures 13(c) and (d), the ineffective lengths are more than those of the figures (a) and (b). In other words, a wider inter-fiber spacing generates a more ineffective length. This may be inconsistent with the experimental result, but it should be noted that a stress concentration around a broken fiber also depends on inter-fiber spacing. As shown in the figures, the stress concentration increased when the inter-fiber spacing is small. As a result the fiber(s) adjacent to a broken fiber would be broken more easily than the fibers with a wide inter-fiber spacing. Due to this, a source of stress concentration consisting of fiber breakage points is formed, as shown in the photographs of Figure 6. Figures 13(e) and (f) show the effects of 2-fiber and 3-fiber breakage on the fiber stress distribution in the composite. The results show that as the number of fiber breakage is increased, a group of the breakage increases the ineffective length in each broken fiber as well as the degree of stress concentration. The ineffective lengths in the 3-fiber breakage are appreciably larger than those of the broken fibers with a wide inter-fiber spacing as in the figures (c) and (d). If a group of the fiber breakage grows further, the ineffective

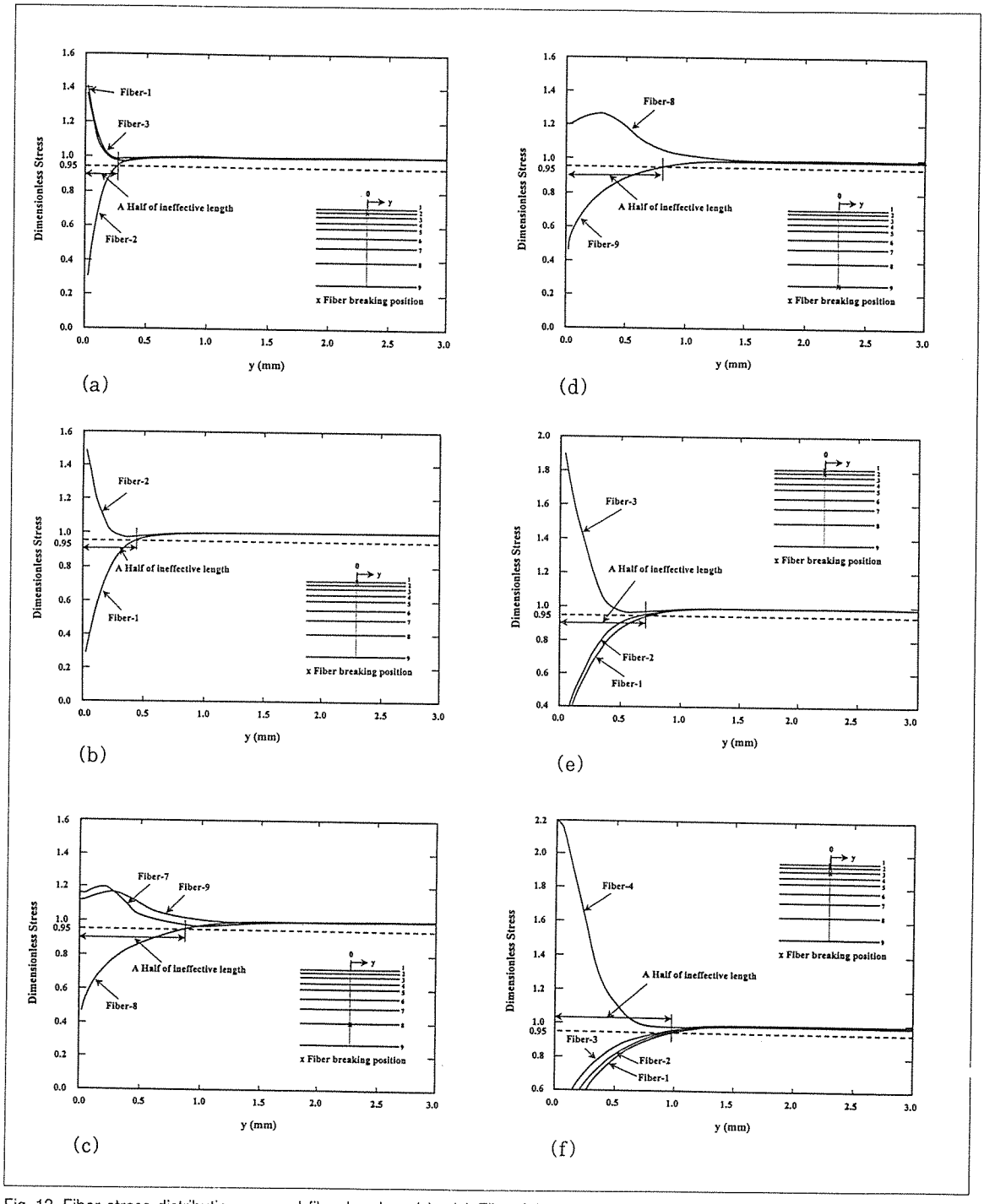

Fig. 13. Fiber stress distributions around fiber breakage(s). (a) Fiber-2 broken; (b) Fiber-1 broken; (c) Fiber-8 broken; (d) Fiber-9 broken; (e) Fiber-1 and -2 broken; (f) Fiber-1, -2 and -3 broken.

lengths would be longer. It is concluded that, therefore, a formation of the successive multi-fiber breakage results in increasing the aspect ratio of the fibers with a narrow inter-fiber spacing. Contrary, since a wide inter-fiber spacing does not bring a large stress concentration, the fibers with it behaves similarly to the SFC.

CONCLUSIONS

A new evaluation method for the interfacial properties of fibrous composites based on fragmentation technique was proposed by using the gradual multi-fiber composite, in which the inter-fiber spacing is gradually changed. Glass fiber and epoxy matrix was chosen as the present model composites. The results showed that as the inter-fiber distance increased, the fragment length and aspect ratio of broken fibers decreased while the interfacial shear strength between the fiber and matrix increased. If the reciprocal of the inter-fiber distance is taken into the above relations, both the aspect ratio and interfacial shear strength were saturated at the low inter-fiber distances. This means that the gradual multi-fiber composite can estimate an upper bound in aspect ratio and a lower bound in interfacial shear strength, while the single fiber composite shows a lower bound in aspect ratio and an upper bound in interfacial shear strength. It was concluded that this fragmentation test is a new method for composite evaluation, since reducing a difference between these two bounds is effective for composite strengthening. In addition an elastoplastic finite element analysis was carried out to estimate fiber stress distributions around fiber breaks. The result showed that a formation of successive multi-fiber breakage increases fragment length or aspect ratio of the broken fibers with a narrow inter-fiber spacing.

FOOTNOTE

*1. As the fiber starts to break from the weakest one, the average of the minimum distribution in the Weibull distribution function is appropriate to its strength level. The average, $\overline{\sigma}$ is given as follows;

$$\overline{\sigma} = N^{-1/m}\sigma_o \Gamma\left(1+\frac{1}{m}\right)$$

where N is the number of fibers (N=9).

ACKNOWLEDGMENT: This work was financially supported by Regional Research Center for Aircraft Parts Technology (ReCAPT) of KOSEF

REFERENCES

1. Sanadi, A. R. and Piggott, M. R., "Interfacial effects in carbon-epoxies", Journal of Materials Science, Vol. 20, 1985, pp.431-437.

2. Park, J. M. and Lee, S. I., "Interfacial aspects of fiber reinforced brittle/ductile matrix composites using micromechanics techniques and acoustic emission", Polymer (Korea), Vol. 21 No. 4, 1997, pp.689-700.

3. Park, J. M., Subramanian, R. V. and Bayoumi, A. E., "Interfacial shear strength and durability improvement by silanes in single-filament composites specimens of basalt fiber in brittle phenolic and isocyanate resins", Journal of Adhesion Science Technology, Vol. 8, 1994, pp.133-150.

4. Park, J. M., Lee, J. O. and Park, T. W., "Improved interfacial shear strength and durability of single carbon fiber reinforced isotatic polypropylene composites, using water-dispersible graft copolymer as a coupling agent", Polymer Composites, Vol. 17, 1996, pp.375-403.

5. Park, J. M. and Subramanian, R. V., "Effects of silane coupling agents on internal reinforcement of wood by E-glass basalt fibers", Journal Adhesion Science Technology, Vol. 5, 1991, pp.459-469.

6. Marshall, D. B. and Oliver, W. C., "An introduction method for measuring residual stress in

fiber reinforced ceramics", Materials Science and Engineering, Vol. A126, 1990, pp.95-103.

7. Grubb, T. and Li, Z. F., "Single-fiber polymer composites: Part I Interfacial shear strength and stress distribution in the pull-out test", Journal of Materials Science, Vol. 29, 1994, pp.189-202.

8. Kelly, A. and Tyson, W. R., "Tensile properties of fiber-reinforced metals: Copper/tungsten and copper/molybdenum", Journal of Mechanical Physics Solids, Vol. 13, 1965, pp.329-350.

9. Wimolkiatisak, A. S. and Bell, J. P., "Interfacial shear strength and failure modes of interphase-modified graphite-epoxy composites", Polymer Composites, Vol. 10, 1989, pp.162.

10. Drzal, L. T., Rich, M. J., Koenig, M. F. and Lloyd, P. F., "Adhesion of graphite fibers to epoxy matrices", Journal of Adhesion, Vol. 16, 1983, pp.133-151.

11. Li, Z. F., Grubb, D. T. and Phoenix, L., "Fiber interaction in the multi-fiber composite fragmentation test", Composite Science Technology, Vol. 54, 1995, pp.251-266.

12. Kim, J. K. and Mai, Y. W., "Stress transfer in the fiber fragmentation test", Journal of Materials Science, Vol. 30, 1995, pp.3024-3023.

13. Accorsi, M. L., Pegoretti, A. and Dibenedetto, A. T., "Dynamic analysis of fiber breakage in single-and multiple-fibre composites", Journal of Materials Science, Vol. 31, 1996, pp.4181-4187.

14. Van Den Heuvel, P. W. J., Peijs, T. and Young, R. J., "Analysis of stess concentration in multi-fibre microcomposites by means of Raman spectroscopy", Journal of Materials Science Letters, Vol. 15, 1996, pp.1908-1911.

15. Weibull, W., Journal of Applied Mechanics., Vol. 18, 1951, pp.293-297.

16. Patankar, S. N., "Weibull distribution as applied to ceramics fibres", Journal of Materials Science Letters, Vol. 10, 1991, pp.1176-1181.

17. Goda, K., Park, J. M. and Netravali, A. N., "A new theory to obtain weibull fibre strength parameters from a single-fibre composite test", Journal of Materials Science, Vol. 30, 1995, pp.2722-1728.

18. Wu, H. F. and Netravali, A. N., "Weibull analysis of strength-length relationships in single Nicalon SiC fibres", Journal of Materials Science, Vol. 27, 1992, pp.3318-3324.

19. Goda, K. and Fukunaga, H. J., "The evaluation of the strength distribution if silicon carbide and alumina fibres by a multi-model weibull distribution", Journal of Materials Science, Vol. 21, 1986, pp.4475-4480.

20. Phoenix, S. L. and Sexsmith, R. G., "Clamp effects in fiber testing", Journal of Composite. Materials, Vol. 6, 1972, pp.322.

21. Goda, K., Hamada, J. and Fukunaga, H., JSME International Journal, Vol. 38A, 1995, pp.616.

22. Asaoka, K. and Niura, I., Journal of Japan Institute Metals (in Japanese), Vol. 40, 1976, pp.644.

23. Hedgepeth, J. M., "Stress concentration in filamentary structures", NASA Technology Note, Vol. D-882, 1961, pp.1-30.

24. Rosen, B. W., "Tensile failure of fibrous composites", AIAA Journal, Vol. 2, 1964, pp.1985-1994.